POLAR COLOR MOSAIC PRODUCTION FROM KAGUYA MI DATA. H. Sato[1], S. Goossens[2], M. Ohtake[1], Y. Daket[3], [1]Japan Aerospace Exploration Agency, 3-1-1 Yoshinodai, Chuo-ku, Sagamihara, Kanagawa, Japan (sato.hiroyuki@jaxa.jp), [2]CRESST, University of Maryland, Baltimore County, Baltimore, MD, USA, [3]ARC-Space, the University of Aizu, Japan.

Introduction: During up to 10 months of the actual observation period, SELENE (Kaguya) Multiband Imager (MI) has achieved over 3400 orbital observations that cover ~95% of the lunar surface. Due to the spacecraft's operation in polar orbit, the observation density of the MI increases toward the pole with significant numbers of repeated observations. The mosaic products from multiple observations (for each pixel) have a higher signal-to-noise ratio (S/N) and reduced color artifacts compared to the one from single observation. The preliminary product of MI north-polar mosaic from the repeated observations by [1] was successful but including systematic artifacts due to the low accuracy of spacecraft's position information. Recently [2] improved the Kaguya's SPK that will improve the coordinates of all the Kaguya observations. Minimizing the geographically mismatched images improves the S/N and photometric normalization by accurate calculations of incidence (*i*), emission (*e*), and phase (*g*) angles. Here we derived a new MI polar color mosaic using the new SPK and evaluated the accuracy of derived reflectance.

Methodology: We used the MI images (9 bands from 415 to 1550 nm; ~20 m/pixel in visible, ~62 m/pixel in NIR)[3] with the center latitude of each image above 80°S (16,762 images, Fig. 1), acquired from November 2007 to Jun 2009. The DN values of all images were radiometrically calibrated to the radiance factor (***I/F***) [4]. The pixel coordinates were derived by SPICE toolkit [5] with the new SPK [2].

The ***i*** and ***e*** angles were computed based on the local topography from Lunar Orbiter Laser Altimeter (LOLA) gridded data records (20 m/pixel) [6]. From the coordinate of each pixel and the locations of the spacecraft and the Sun at the time of each observation, we computed the ***i***, ***e***, and ***g*** angles.

Next, we calculated the photometric parameters using Hapke model [4]. Instead of deriving the Hapke parameter maps [7], we derived a single set of parameters to obtain enough angle variations of ***i*** and ***e***. Then we derived the photometrically normalized ***I/F*** (***nI/F***) by the single parameter set. Since the south polar region is dominantly the highland region, we assumed that our studied area is photometrically uniform. For the sampling site of the Hapke parameter calculation, we selected a rectangular region (Fig. 1 red box) where there are no extensive immature ejecta deposits.

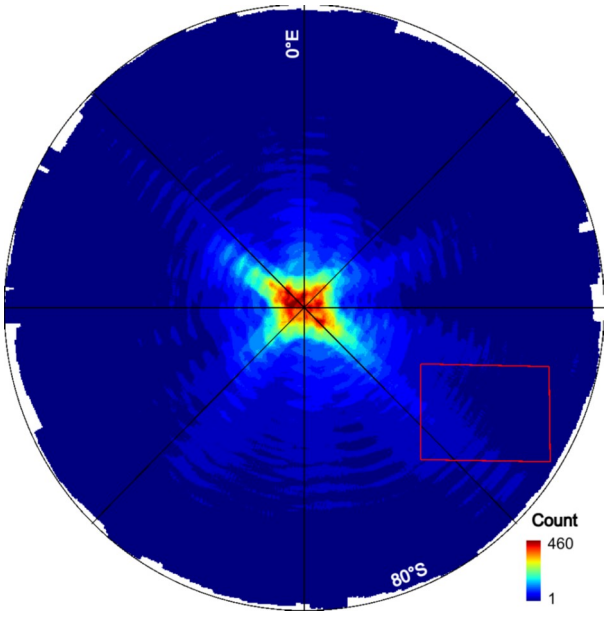

Figure 1. Number of repeated observations by the MI above 80°S. Black lines indicate latitude 80°S; longitude from 0°E to 270°E (clockwise). Red box outlines the sampling site for the Hapke parameter calculation.

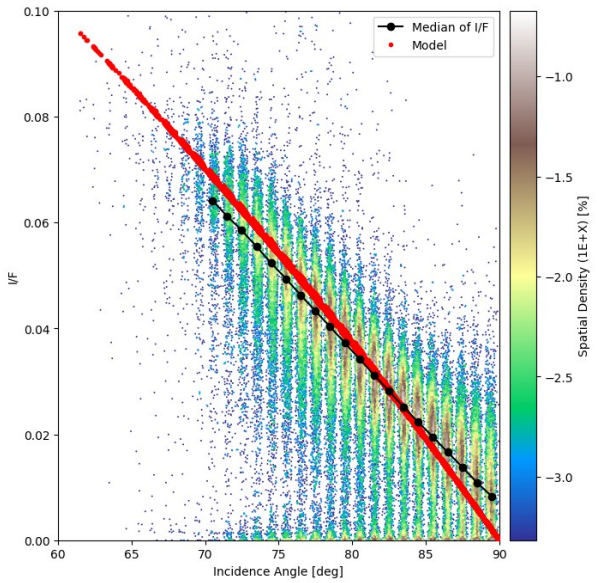

Figure 2. Density plot of the incidence angle (***i***) vs ***I/F*** in 1550 nm band. Red and black lines correspond to the model fit and the median of ***I/F*** in each 1° bin. Down-sampling by binning of ***i***, ***e***, and ***g*** angles for each MI image before mixing all the MI observations acquired inside the sampling site (Fig.1 red box) has resulted in the vertical stripes.

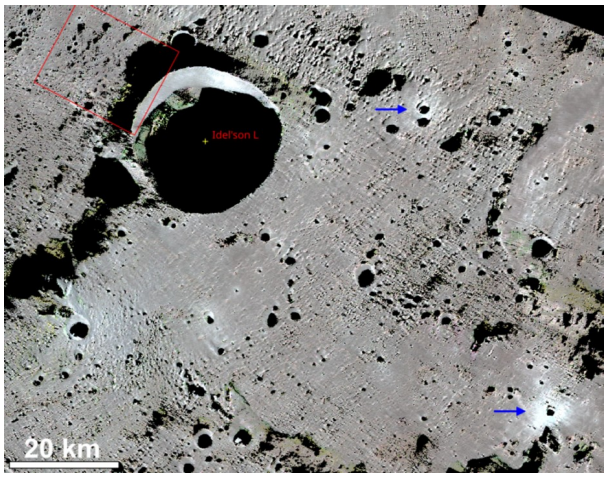

Figure 3. MI median mosaic in a form of RGB color composite (R:1550 nm, G:1000 nm, and B: 900 nm). Red box in Fig. 1 indicates the spatial extent of this figure, and red box in this figure displays the location of Fig. 4. Blue arrow indicates the fresh crater ejecta.

From all the overlapping observations we computed a median of ***nI/F*** for each pixel value of the final mosaic product (hereafter called "median mosaic").

Results: The number of repeated observations within the south-pole region (>80°S) ranged from 1 to 460 (Fig. 1; 26.3 on average). The pole has the highest density due to Kaguya's polar orbit operation.

The curve-fit on the observed ***I/F*** for the Hapke parameter calculation (Fig. 2) achieved a small mean difference of 0.0001 (0.4% of averaged ***I/F***). The offset relative to the median of each bin (Fig. 2 black line) is caused by local undulations unresolved by the topography data, which add the scatters and increase the averaged level of ***I/F*** at ***i*** close to 90°. The derived free parameters

The RGB composite map of the MI median mosaic (Fig. 3) exhibits no topographic relief (except the sharp shadows) nor color artifacts, indicating that the photometric normalization was performed with enough accuracy. The high reflectance of immature ejecta of the small craters (~1.5 km in diameter, Fig. 3 blue arrow) are clearly displayed, demonstrating the potential for the albedo studies in the polar regions. The multiple wrinkles extending from lower-left to upper-right in the image (perpendicular direction to the pole) are possibly the small topographic undulations that cause subpixel shadows frequently.

Discussion: The sharp topographic boundaries in the median mosaic (Fig. 3) indicates that the new SPK has enough accuracy to match the pixel-to-pixel of multiple MI images acquired in different orbits.

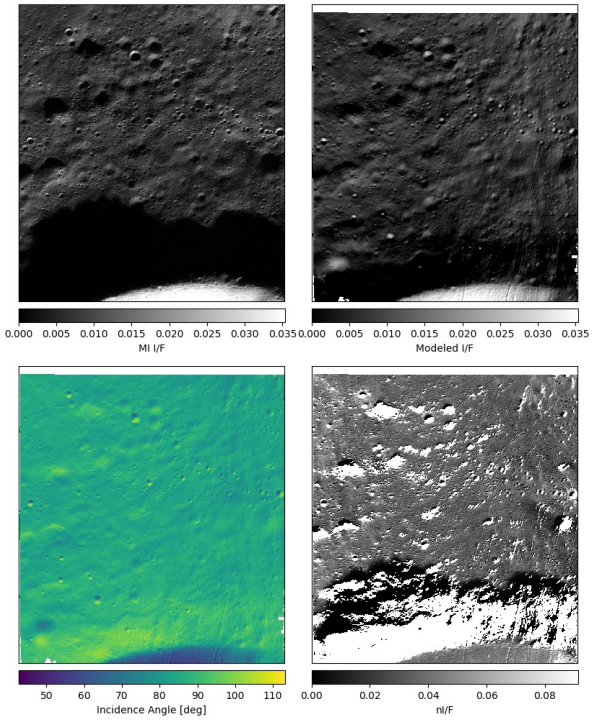

Figure 4. Sample MI image (ID: 03_04747S848E1173) in ***I/F*** (upper left), modeled ***I/F*** derived by Hapke model (upper right), incidence angle layer (lower left), and ***nI/F*** (lower right). Southern rim of Idel'son L crater is shown in the bottom of all images. In the bottom right panel, the dark zone above the shadowed region (white null pixels) corresponds to abnormal ***nI/F*** area, caused by the unpredicted shadow.

The shadows cast from the topographic summits and ridges (e.g., crater rim) often result in inaccurate ***nI/F***. The southern rim of Idel'son L crater, for example, makes a long shadow (~7.2 km, Fig. 4 top left). These shadows are not predictable from the incidence angles. Thus the modeled ***I/F*** (Fig. 4 upper right) is unable to recreate accurate shadow areas, resulting in the low ***nI/F*** zone along the crater rim. It is hard to detect such shadowed areas by setting thresholds on ***nI/F*** because the shadows are vaguely-outlined by indirect lighting from the nearby slopes. The effect of the Sun disk fraction, which is emphasized with shadow length, also blurs. An illumination simulation by ray-tracing will help to predict the shadowed regions accurately behind the mountains.

References: [1] Sato et al. (2018) *New Views of the Moon 2 – Asia*, abstract #6011. [2] Goossens et al. (2020) *Icarus* 336, 113454. [3] Kodama, S. et al. (2010) *Space Sci. Rev.*, v154, 1-4, p79-102. [4] Hapke, B. (2012) *Cambridge Univ. Press*, NY. [5] Acton, C. H. et al. (1996) *Planet. Space Sci.*, v44, p65-70. [6] Smith et al. (2010) *GRL*, 37(18). [7] Sato et al. (2014) *JGR-Planets*, 119(8), 1775–1805.